Journal of Physical Chemistry & Biophysics
ISSN: 2161-0398

Chihaoui et al., J Phys Chem Biophys 2016, 6:3
DOI: 10.4172/2161-0398.1000216

Research Article Open Access

A New Mononuclear Complex: Structure, Vibrational (FT-IR and Raman), Hirshfeld Surfaces Analysis, Electrical Properties and Equivalent Circuit

Nejla Chihaoui, Besma Hamdi*, Abdelhamid Ben Salah and Ridha Zouari

Laboratory of Materials Science and Environment, Faculty of Sciences of Sfax, University of Sfax, Tunisia, BP 1171, 3000 Sfax, Tunisia

Abstract

The present paper aims to develop the synthesis, crystal structure, and properties of $Zn(C_7H_5NO_4)Cl_2.H_2O$ compound investigated by vibrational study, thermal analysis and dielectric measurements. The single crystal X-ray diffraction investigation reveals that the studied compound crystallizes in the orthorhombic system with space group Pnna according to the following lattice parameters: a=13.8816(4) Å, b=10.3602(3) Å, c=7.8967(2) Å and Z=4. The presence of the key functional groups in the molecule has already been confirmed by Fourier transform infrared (FT-IR) analysis. Thermal behaviour of this sample, studied by TGA and DSC exhibit two anomalies at 345 and 386K. The hydrogen bonding plays a significant role in the stabilization of the structure. Such a parallel displaced structure has also a contribution from π-σ non-covalent interactions (C-H…π and C-O…π stacking between the C-H groups and C-O groups with the benzene rings). The dipicolonic acid (2,6-pyridinedicarboxylic acid) ligand coordinated to the Zn(II) ions through a nitrogen atom of pyridine ring, two oxygen atom of carboxylic group and two chloride atoms as a tridentate ligand. Hirshfeld surface analysis of the intermolecular interactions in crystal structures have been used to scrutinize molecular shapes. The characteristic features of ^{13}C solid state CP/MAS-NMR applications showed five isotropic resonances, confirming the structure determined by XRD. Its dielectric properties as a function of temperature and frequency in the ranges 298-418 K and 209 Hz-5 MHz are measured. The Cole-Cole (Z' versus Z'') plots are analyzed by fitting to an equivalent electrical circuit model, consisting of a circuit elements; grain, grain boundary, electrode-solid interface polarization and Warburg resistance. Each circuit elements is formed by a parallel combination resistance (R) and constant phase elements (CPE). The grain conductivity as well as the activation energy depending to of temperature, via impedance technique, besides the activation energy due to relaxation time as function of temperature, have been studied showing two anomalies, which are also detected by the TGA and DSC. They could be explained by not only a phase transition and reorientation hopping between equivalent sites at 343K but also the disappearance of the water molecule of the structure at 388K.

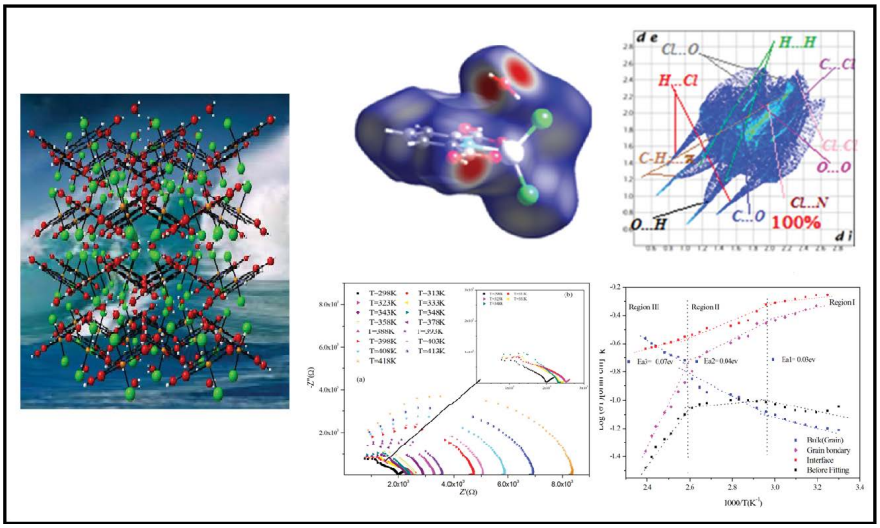

Keywords: Dipicolinic acid; Spectroscopic; Hirshfeld surface analysis; Differential scanning calorimetry (DSC); Electric properties

Introduction

Hybrid compounds offer attractive opportunities to combine useful properties of both organic and inorganic simples within a single molecular scale composite. On the one hand, these salts offer, scientifically and technologically significant chances in different areas of catalysis, optical properties, biology, magnetic functional materials. On the other hand, they may contribute to higher electrical mobility (as a result of the strong covalent bonding within these systems) [1-4]. Halogenometalate hybrid compounds based on elements of

***Corresponding author:** Besma Hamdi, Laboratory of Materials Science and Environment, Faculty of Sciences of Sfax, University of Sfax, Tunisia BP 1171, 3000 Sfax, Tunisia, Tel: +21625493020; E-mail: bh_hamdi2006@yahoo.fr

Received March 30, 2016; **Accepted** April 30, 2016; **Published** May 08, 2016

Citation: Chihaoui N, Hamdi B, Salah AB, Zouari R (2016) A New Mononuclear Complex: Structure, Vibrational (FT-IR and Raman), Hirshfeld Surfaces Analysis, Electrical Properties and Equivalent Circuit. J Phys Chem Biophys 6: 216. doi:10.4172/2161-0398.1000216

transition (II) ions [5-7] prove to have a significant weight to fabricate low-cost electronic devices (as Thin Film Transistor or Organice-Inorganic Emitting Diode) [8,9]. Among the most frequently used of polydentate ligands which have the ability with bond to several metal centers, dipicolinic acid ($C_7H_5NO_4$, 2,6-pyridinedicarboxylic acid) is a well-known that occurs in many natural compounds exhibiting various biological functions and potential pharmacological activities. 2,6-pyridinedicarboxylic The ligand containing N and O polydentate donors, which pave the way provide great advantages for assembling compounds with new structures [10-14]. The dipicolinic acid 'dpc' ligand with Zn (II) ions has commonly 1 or 2 coordination modes. In one coordination mode, a single planar dpc ligand associates in the equatorial plane of a Zn (II) cation with other ligands such as H_2O or pyridine-based heterocycles, which occupy the remaining sites. This leads to the formation of square pyramidal or octahedral coordination geometry [15,16] or two perpendicularly coordinated planar dipicolinic molecules generating distorted octahedral coordination geometry [17,18]. Our central focus is on the determination of spectroscopic and structural properties of a new complex containing: dipicolinic cation together with zinc chloride ligand, namely $Zn(dpc)Cl_2.H_2O$. Moreover, we are equally interested in the study of the interactions between molecular coordination chemistry: derivatives of transition metal and aromatic pyridine polycarboxylates. Hirshfeld surfaces which help us investigate intermolecular interactions structure is constructed by dividing space into regions in which the electron density of the sum of spherical atoms in the crystal packing into a single (3D) surface. Moreover, the (3D) surface can be reduced into a (2D) fingerprint plot, which summarizes the complex information that atoms are genuinely interacting with one another present in crystals [19-21]. In addition our work presents the results of the spectroscopic analysis, MAS-NMR ^{13}C characterization and the differential scanning calorimetry. The results of the simulation of the complex impedance are also reported by an equivalent circuit and conductivity measurements according to the conduction mechanism in the temperature range 298-418 K and the frequency range 209 Hz-5 MHz for $Zn(dpc)Cl_2.H_2O$.

Experimental Analysis

Synthesis of $Zn(dpc)Cl_2.H_2O$ compound

The $Zn(dpc)Cl_2.H_2O$ crystal was prepared in stoichiometric condition by dissolving $ZnCl_2$ (0.73 mmol, 99%) and 2,6-pyridine dicarboxylic acid (1.49 mmol, 97%) in concentrated HCl solution (1 ml, 38%). The solution was left to evaporate slowly at room temperature. After a few months, an observed precipitate was separated by filtration, collected and dried to give colorless parallelepiped-shaped mono-crystals. The material formula was determined by chemical elementary analysis and confirmed by structural refinement. A single crystal chosen was used for x-ray crystallography studies.

Characterization

The FT-IR spectra were recorded in the range of 4000-400 cm^{-1} on a "Nicole Impact 410 FT-IR" spectrophotometer as a function of temperature, using a sample and KBr must be ground. The pellet was prepared by mixing 15 mg of powder sample with 300 mg of KBr (The KBr was dried at 383 K) compressing the whole into a disk. The heating of all 10 K of the $[Zn(dpc)Cl_2].H_2O$, pellet in the temperature range of 298-398 K was performed by an air-atmosphere Spectrac heating cell. The Raman spectra of powder sample was recorded between 50 and 4000 cm^{-1} using LABRAMHR 800 triple mono-chromator instrument using the 514.5 nm line spectra-physics argon ion laser. The thermal analyses (TGA) were carried out using a Perkin Elmer Pyris 6 TGA thermogravimetric analyser. The differential scanning calorimetry analysis was obtained using a (SETARAM DSC 131-ks) instrument between 250K and 520 K at the heating rate of 5 K min^{-1}, with a powder sample of 20.3 mg in weight placed in a hermetic aluminum cell in a nitrogen atmosphere. The CP/MAS-NMR experiment was conducted at room temperature on a Bruker MSL 300 spectrometer operating at 75.48 MHz for ^{13}C. The powdered sample was packed in a 4 mm diameter rotor and allowed to rotate at speeds up to 10 kHz in a Doty MAS probe head. During the whole acquisition time, the spinning rate of the rotor was locked to the required value thanks to the Bruker pneumatic unit which controls both bearing and drive inlet nitrogen pressures. The spectra were acquired by the use of cross-polarization for proton with 5 ms contact time. All chemical shifts (δ) were given with respect to tetramethylsilane, according to the IUPAC convention, i.e., shielding corresponds to negative values. Spectrum simulation was conducted using Bruker WINFIT software [22]. The chemical analysis of zinc and chloride atoms was performed to confirm the formula determined by the structural refinement [23]. The density of this compound was measured at room temperature by picnometry method.

Electrical measurements

The impedance spectroscopy analysis was obtained from pressed pellet discs of about 8 mm in diameter and 1.1 mm in thickness using a hydraulic press at a pressure of 4×10^4 Nm^{-2}. The complex impedance was performed in the frequency range of 209 Hz-5 MHz using the TEGAM 3550 ALF impedance, automatic bridge monitored by a microcomputer, over the temperature range of 298-418 K.

Crystal data and structure identification

The experimental conditions used for the single crystal diffraction data collection are reported in Table 1. The data were collected on a BruKer AXS CCD area detector system equipped with monochromatic MoKα radiation (0.71073 Å) at 293(2) K. Lattice parameters were found from the setting angles of 8721 reflections in the $2.9 \leq \theta \leq 28.9°$. The crystal compound has a prismatic form has a prismatic form with a size of about $(0.42 \times 0.22 \times 0.13)$ mm^3. The empirical absorption corrections are based on multi-scan. The structure was solved using the Patterson method with the SHELXS 86 program [24]. The refinement was carried out by full-matrix least squares methods SHELEXL 97 program [25] and converged to an acceptable final agreement factor. All hydrogen atoms were refined isotropically. The last cycle of refinement included the atomic coordinates for all atoms, anisotropic thermal and isotropic thermal parameters, whose values are listed in Tables S1 and S2, respectively. The structure graphics were created with ORTEP [26] and DIAMOND [27] (Figure 1).

Results and Discussion

Description of the structure

The title compound crystallizes in the orthorhombic system, *Pnna* space group, with unit cell dimensions, *a*=13.8816(4) Å, *b*=10.3602(3) Å and *c*=7.8967(2) Å. The asymmetric unit of $Zn(dpc)Cl_2.H_2O$ shown in Figure 1 reveals that the organic part is related to the inorganic part by dative covalent bonds (coordination bonds). There are three basic relationships. It is the interaction between the empty orbital of zinc cation and a lone pair of the nitrogen, the relationship between the empty orbital of zinc cation and the electrons from the nitrogen lone pair, on the one hand, and the electrons from lone pairs of two oxygen atoms of two carboxylic acids groups of tridentate ligands of

Crystal data	
Empirical formula	$ZnC_7H_3NCl_2.H_2O$
Formula weight	321.43
Crystal system	Orthorhombic
Space group	Pnna
Hall symbol	-P 2a 2bc
Unit cell dimensions	
a (Å)	13.8816(4)
b (Å)	10.3602(3)
c (Å)	7.8967(2)
Volume (A^3)	1135.67(5)
Z	4
D_{calc} (mg m^{-3})	1.88
D_{mes} (g.cm^{-3})	1.9(2)
Absorption coefficient (mm^{-1})	2.636
F(000)	640
Crystal dimensions (mm)	0.42 × 0.22 × 0.13
Crystal color	Prism, colorless
θ Range for data collection (°)	2.9–28.9
Data collection	
Reflections collected	8721
Independent reflections	1506
Reflections with I > 2σ(I)	1090
Limiting indices	h = -17→15
	k = -13→13
	l = −9→10
Absorption correction:	multi-scan (North, Phillips & Mathews (1968))
	T_{min} = 0568
	T_{max} = 0.666
Refinement	
Refinement method	Full-matrix least– Squares on F^2
R [F^2 > 2r(F^2)]	0.034
wR(F^2)	0.096
Goodness-of-fit on F^2	S = 1.030
Extinction coefficient	0.000
$\Delta\rho_{max}$ (eÅ^{-3})	0.35
$\Delta\rho_{min}$ (eÅ^{-3})	-0.51
CCDC deposit number	977198
CCD area detector diffractometer adiation	
source: fine-focus sealed	
tube Graphite ϕ and ω scans	

Table 1: Summary of crystal data, intensity measurement and refined parameters of $Zn(dpc)Cl_2.H_2O$ compound.

organic part, on the other hand. It is also the interaction with two chlorine atoms. The Zn (II) center metal binding site has a similar pent-coordinate model, and an NO_2Cl_2 donor set at Zn (II). It is composed of a tertiary amine nitrogen atom (pyridine N), two carboxylate O atoms and two chlorine Cl atoms as shown by the lengths of bonds Zn-Cl distance of 2.204 (3) Å, Zn-N distance of 2.047 (3) Å and Zn-O distance of 2.313 (18) Å. the results are more or less compatible to a similar system [28]. The bond lengths and angles of Zn-O-N, Zn-Cl-Cl, Cl-Zn-O and Zn-O-N are listed in Table S3. Three atoms, two chlorine atoms and a nitrogen atom, whose angles equal 120.19° and 118.22° (equatorial positions), are directly bonded to the zinc central atom to form a plane. The two oxygen atoms remain above and below the plane. A deflection angle implies that this coordination structure is a distorted trigonal-bipyramid. To confirm this geometry, a structural index τ has been calculated by the following formula [29]. τ=47%, which indicates that Zn (II) ion center in the complex form a distorted trigonal bipyramid coordination to a greater or less extent. The ideal trigonal-bipyramidal geometry is indicated by the basal angle (120°) resulting a τ=1. The intermolecular forces, can be a rather complex process, they are consist of the hydrogen bonding of the type O-H···O, C-H···O and O-H···Cl and ion pairing (Figure 2). The hydrogen bonding is displayed in Table 2. Other non-covalent interactions formed, which are due to the presence of conjugated system of double bonds are C-H…π and C-O…π constructed between the C-H groups and C-O groups with the aromatic rings. These bonds are shorter than 3.9 Å (Figure S1) [30].

Hirshfeld surface analysis

Hirshfeld surface analysis [21] is a method with a different design philosophy from traditional structure study: it treats molecular interactions in cells. Such an analysis of all existing interactions and

D-H …A	*D-H*	*H …A*	*D-A*	*D–H–A*
O1-H1…O3	0.8200	1.8600	2.669(2)	170.00
O1-H1…O3	0.8200	1.8600	2.669(2)	170.00
O3-H1 …Cl1	0.85(3)	2.28(3)	3.0847(18)	158(3)

Symmetry codes: (ii) x, y, z-1; (iii) –x+1/2, -y+1, z-1; (iv) –x+1/2, y+1/2, -z+1/2.

Table 2: Main inter–atomic distances and bond angles involved in the hydrogen bonds of $Zn(dpc)Cl_2.H_2O$ crystal.

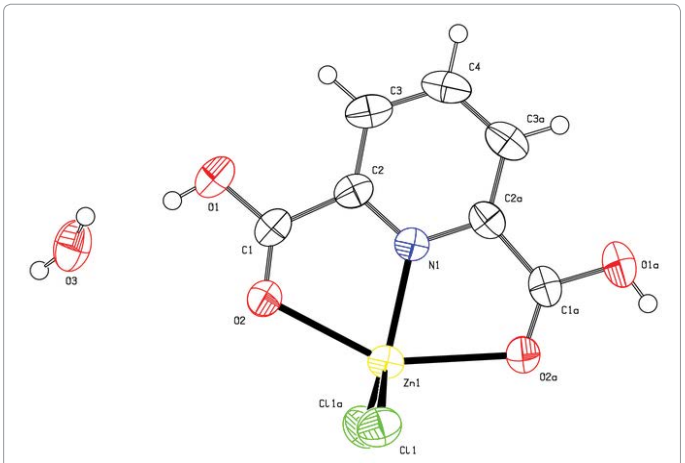

Figure 1: The asymmetric unit of the $Zn(dpc)Cl_2.H_2O$ compound. Ellipsoid represented at 50% probability level; only hydrogen atoms are not labeled.

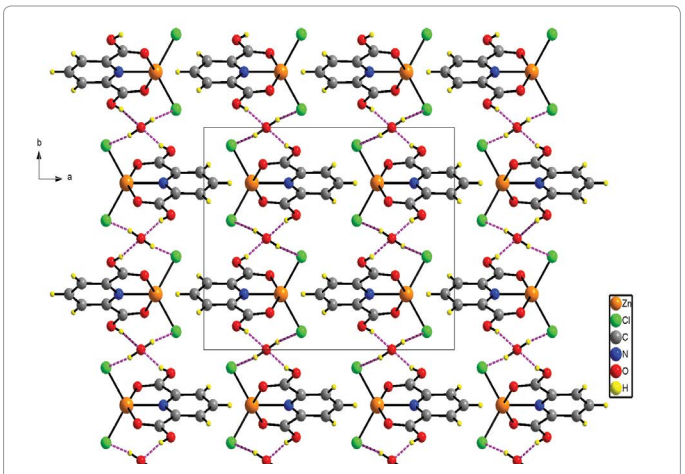

Figure 2: Packing diagram of the $Zn(dpc)Cl_2.H_2O$ compound in the (*b a*) plane. Dotted lines represent hydrogen bonds.

different structural information will be obtained. Information about interactions possibly is indicated by using of surface color-coding differentiation. Hirshfeld surface (HS) analysis is almost constantly accompanied by 2D Fingerprint Plots (FP) [31]. The Hirshfeld surfaces of the title complexes are illustrated in Figure 3 showing surfaces that have been mapped over, d_{norm}, d_e and curvedness shape index. The information regarding intermolecular interactions which are presented in Table 2 is visible by the spots on the Hirshfeld surfaces. In such plots, relative areas of points, which can be attributed to certain close contacts, are identified and their percentage share is provided. The Hirshfeld surfaces of the complex are illustrated in Figure S2, showing surfaces that have been mapped over a d_{norm}. The normalized contact distance (d_{norm}) calculated using the both d_e and d_i and the van der Waals (vdW) radii of atoms. and showed circular depressions (deep red) visible in front and back surface are indicative of hydrogen bonding contacts and other visible spots are due to H…Cl, H…H, O…H…contacts (Figure S2).

$$d_{norm} = \frac{d_i - r_i^{vdw}}{r_i^{vdw}} + \frac{d_e - r_e^{vdw}}{r_e^{vdw}}$$

where d_e and d_i are the distances from the Hirshfeld surface to the nearest atom outside (external) and inside the surface.

Three-dimensional (3D) Hirshfeld surface maps are generated with d_{norm} has been visualized using a red-white-blue color scheme; shorter contacts, vdW contacts, and longer contacts, respectively, and two dimensional (2D) fingerprint plots generated using d_e and d_i. Hirshfeld surface analysis and the attribution were performed using Crystal Explorer 3.0 software [32]. The surfaces are represents as transparent to allow visualization of the complex, around which they were calculated. A diagram of percentage contributions of different intermolecular forces and the (2D) fingerprint plots of the compound indicate different interactions are shown in Figure 4. The O···H / H···O interactions are determined by as two distinct spikes in the fingerprint plot. The Hirshfeld surface do not shows a similar proportion of O…H (14.1%) and at H…O (12, 6%) interactions, which provide information on intermolecular hydrogen bonding. These contacts in this complex can be attributed to C-H···O, N-H···O and O-H···O hydrogen bond interactions manifest in Hirshfeld surfaces as red areas. The O···H interactions are represented by a sharp spike (d_e+d_i ~ 1.70 Å), while the H···O interactions are represented by a comparatively large spike (d_e+d_i ~ 1.73 Å). This is one of the closest contacts in the structures and can be viewed as numerous dark red spots on the dnorm surface. Reciprocal H···Cl / C···H dispersion forces are the second most abundant type of interactions in structures appear as two spikes in the (2D) fingerprint plots. These complementary regions are visible in the fingerprint where one molecule acts as donor ($d_e>d_i$) and other as an acceptor ($d_i>d_e$). The third largest contribution can be found for the H…H interactions, totaling 16.6%, reflecting in the middle of scattered points in the 2D fingerprint plots, exhibit a significant contribution of scattered points at

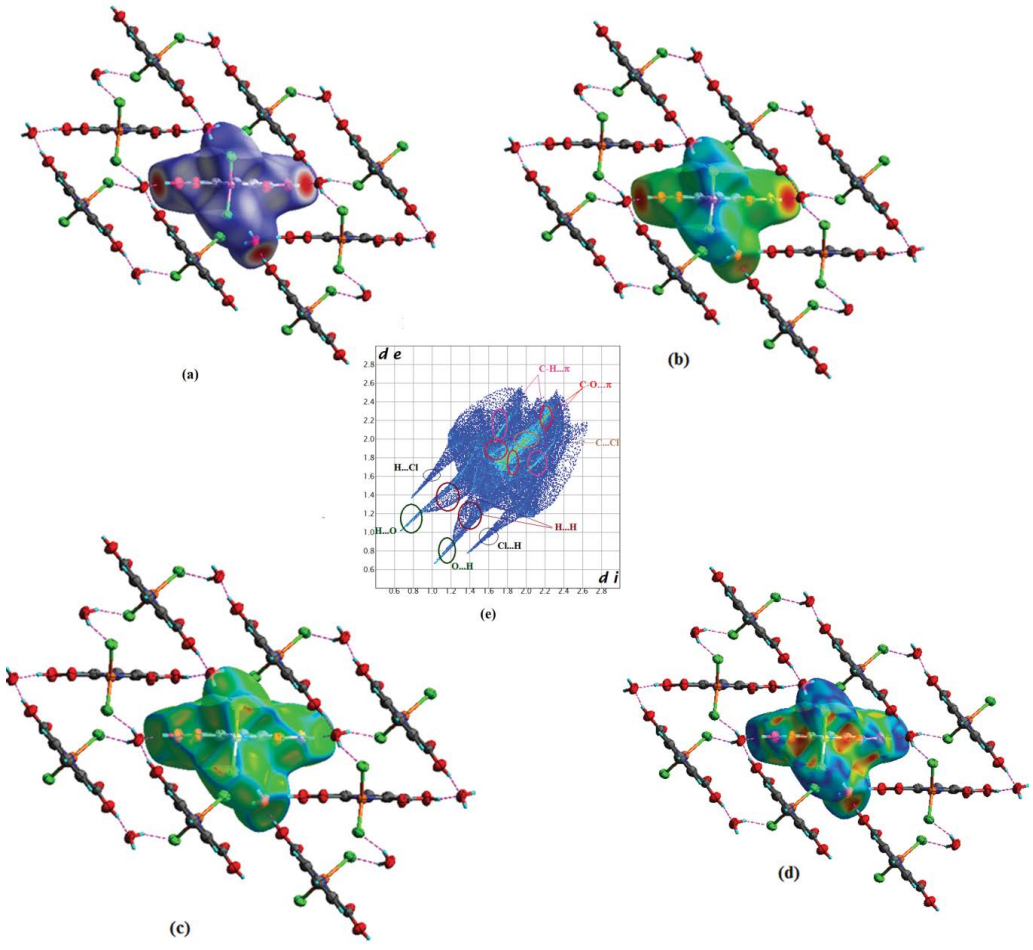

Figure 3: Hirshfeld surfaces mapped with $d_{norm,}$ d_e, curvedness and shape index of $Zn(dpc)Cl_2.H_2O$ complex.

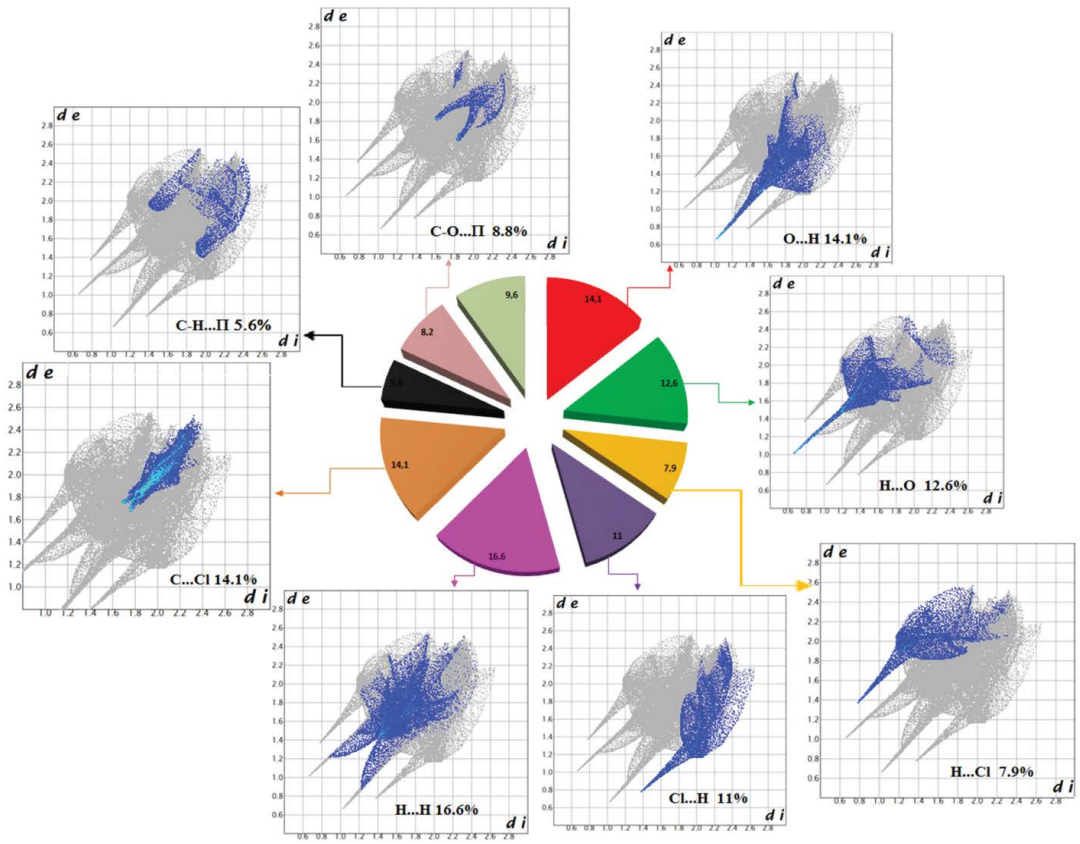

Figure 4: Chematic illustration of decomposed figureprint plots of $Zn(dpc)Cl_2.H_2O$ compound, different colors have been used for the various atom pair contacts.

the fingerprint plots. These are spread only up to (d_e=d_i=1.25 Å). There are a small variance in distribution of C-H···π interactions (confirming the presence of very weak. there are characteristic "wings" which are identified as a result of C-H···π interactions. The wings at the top left (d_i<d_e) corresponds to points on the surface around the C-H donor, whereas that at the bottom right (d_e>d_i) corresponds to the surface around the π acceptor. Also, the structures are stabilized through C-O···π C…Cl interactions which are visible on the de surface as well as in fingerprint plots. Finally, these examples mark the value of Hirshfeld surfaces and in particular, fingerprint-plot analysis for the 'visual screening' and rapid detection of unusual crystal structures features.

FT-IR and FT-Raman spectroscopy

The FT-IR absorption frequencies of the title compound Zn(dpc)$Cl_2.H_2O$ have been identified and compared with those of free ligand (2,6-pyridinedicarboxylic acid). Figure 5 presents the FT-IR spectra of the two compounds at room temperature. Some of the infrared absorption bands of the functional groups can be attributed by comparison with similar compounds. The examination of FT-IR spectrum affects the correlation of absorption bands in the spectrum (b) of $Zn(dpc)Cl_2.H_2O$ compound with the spectra (a) of organic compound, which can be attributed to the chemical environment change of pyridine groups in the $Zn(dpc)Cl_2.H_2O$ compound. This indicates that Zn-O and Zn-N bands appeared in the hybrid at 541 and 452 cm^{-1} [33]. The patterns of the FT-IR spectrum of complex (b) reveal two vibration sets due to the aqua and dipicolinate ligands (Figure 5). The ν(O-H) vibrations belonging to the (H_2O) fragments are observed as two bands at the 3474 and 3423 cm^{-1}. Figure 6 displays the superposition of the FT-Infrared and FT-Raman spectra of the product $Zn(dpc)Cl_2.H_2O$ performed at room temperature between 4000-400 cm^{-1} and 4000-50 cm^{-1}, respectively. Referring to previous works, we attempted to determine the vibrational frequencies of the groups of the organic cation identification [33-35]. The FT-Raman spectrum $[Zn(dpc)Cl_2].H_2O$ recorded between 500 and 100 cm^{-1} is shown in Figure 8. Besides, the peaks of symmetric and asymmetric deformation vibration of Zn-Cl bond in the $[Zn(dpc)Cl_2].H_2O$ appear at 217 and 194 cm^{-1}, respectively [36]. The external vibrations of the organic molecule can be determined by the low wavenumber. The main attempts of bands attribution are gathered in Table 3.

CP/MAS-RMN spectroscopy

The experimental spectrum of ^{13}C nuclear magnetic resonance of $Zn(dpc)Cl_2.H_2O$ between 90 and 270 ppm is presented in Figure 7. The fitting of the experimental spectrum of ^{13}C using Lorentzian and Gaussian functions was performed with the Dmfit program [37]. In this spectrum, five singlets indicating no coupling with zinc nuclei are observed. The peak at lower field, 168.00 ppm, is attributed to C1 and C1a which are carboxylate carbons [38]. Referring to literature studies [39-41], the chemical shifts are reported in Table S4, showing that the high value of chemical shifts 145.23 ppm is assigned to carbons which are ortho to the nitrogen of a pyridine ring. The signals at 141.23, 132.93 and 130 ppm are assigned to three pyridine carbons: C4, C3 and C3a. The red spectrum proves to be in good agreement with accords well with the deconvolution emanating from the experimental results (blue spectrum). These results prove the presence of only one organic cation in the asymmetric unit of the compound in conformity with the X-ray

Modes of vibrations	IR (cm^{-1})	Raman (cm^{-1})
v_{as} *(O-H)*	3540	–
v_s *(O-H)*	3230	–
	3140	
v_{as} *(C-H)*	3070	
	2910	2970
	2850	2878
v_s *(C-H)*	2650	–
	2510	–
v (COOH)	1710	–
δ (O-H)	1624 1596 1470	–
v (C=N)	1364 1250	–
δ (C-H)	1080	1060
ρ (C-H)	855	–
δ (N-H)	640 587	–
δ (C-N)	536 451	330
δ (Zn-N)	602	–
δ (Zn-O)	420	–
v_{as} (Zn-Cl)	–	217
v_s (Zn-Cl)	–	194
v_{as} (Cl-Zn-Cl)	–	133
v_s (Cl-Zn-Cl)	–	102

Table 3: Tentative of assignments of IR and Raman wavenumber in the range 4000-50 cm^{-1} of $Zn(dpc)Cl_2.H_2O$.

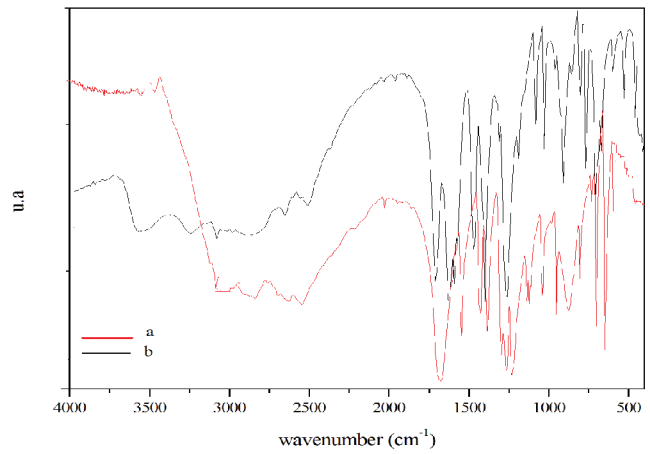

Figure 5: FT-IR spectra of (a): $C_7H_7NO_4$ and (b): $Zn(dpc)Cl_2.H_2O$ at room temperature.

diffraction data. Therefore we conclude that our crystals are pure.

Thermal property

The differential scanning calorimetry (DSC) curve of $Zn(dpc)Cl_2.H_2O$ crystal is presented in Figure 8. An overview of this curve obviously shows the existence of three distinct endothermic peaks; the first at T=345K, the second at T=386K and the third at T=508K. The shapes of the observed scanning anomalies of the first peak suggest the existence of a structural phase transition at 345K (heating). Indeed, no weight loss was detected in TGA at this temperature, which confirms that the observed peak is a transition and the second peak at 386K (heating) corresponds to the evaporation of water molecules. Besides, the TGA curve shows that the compound exhibits one-weight loss observed around 386K. This weight loss equal to 5.2 ± 0.3% corresponds to the release of one structural water molecule, which is in good agreement with the calculated value 5.6 ± 0.3%. These are confirmed by dielectric studies at different temperatures. Furthermore, an endothermic peak occurring at 508K corresponds to the melting process of the $Zn(dpc)Cl_2.H_2O$ complex. To obtain more information on the crystal, a high-temperature infrared study was carried out. Figure S3 shows the superposition of the Infrared spectra in the temperature range of 298-393 K. A progressive variation of the speed (look) of spectra was detected in the zone characterizing the vibrations of the water strain. This variation was observed between the temperatures 298K and 383K. The displacement of certain peaks and the disappearance of others in the field along the low-frequency are also reported. The obtained results are in agreement with those found by our previous DSC and TGA thermal study.

Electric properties

Electrical impedance spectroscopy was used to characterize the $Zn(dpc)Cl_2.H_2O$. This technique utilizes alternating current in the temperature range [298-418K] and the frequency range [209 Hz-5

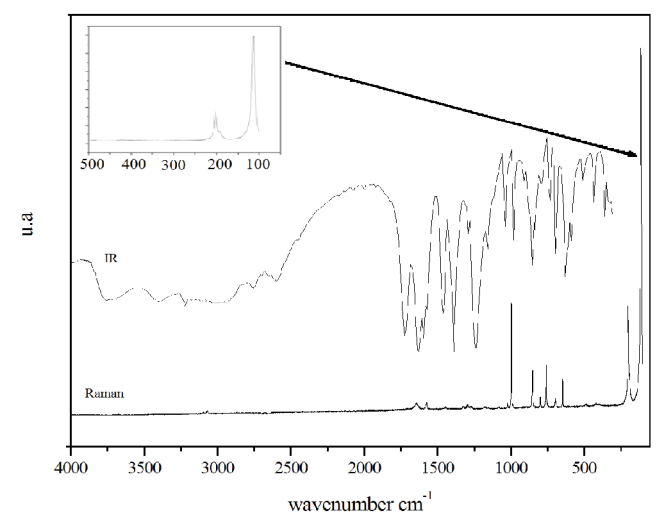

Figure 6: Superposition of FT-IR and the Raman spectra of $Zn(dpc)Cl_2.H_2O.H_2O$ compound at room temperature.

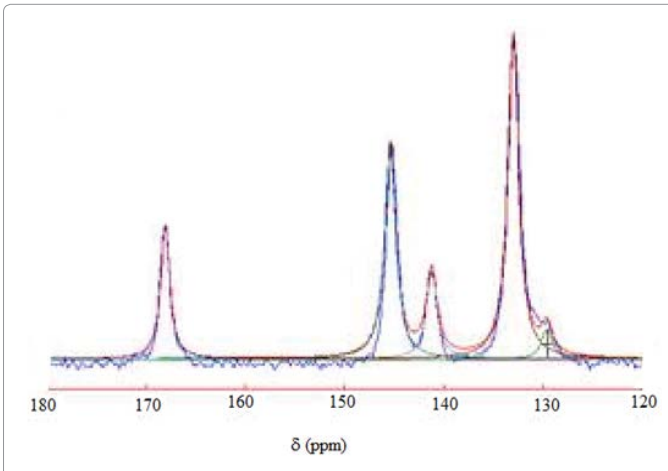

Figure 7: Plots of experimental and fitted curves of the isotropic band of the ^{13}C spectrum of $[Zn(dpc)Cl_2].H_2O$ compound.

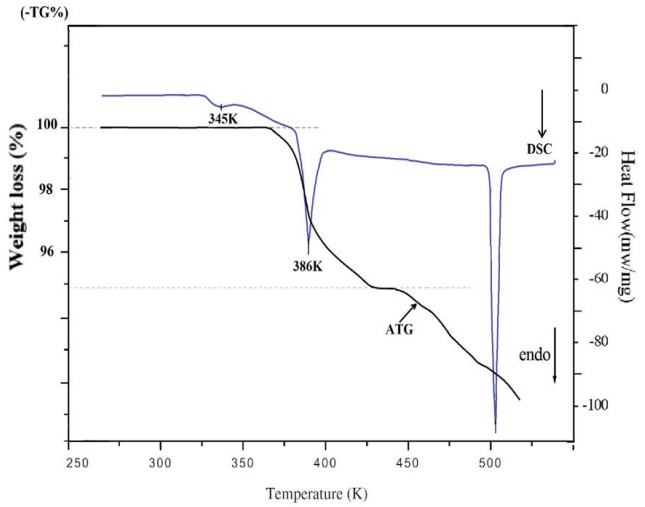

Figure 8: TGA-DSC runs at a rate of 5 k min^{-1} on heating of Zn(dpc)Cl_2.H_2O crystal.

MHz] to determine the activation energies of the conduction and dielectric relaxation processes [42,43]. It is an important technique serving to separate the contributions of electro active regions such as the bulk, grain boundaries, electrode-solid interface and Warburg effects in the frequency domain [41,44,45]. Generally, the data in the complex plane is represented in any of the basic formalisms below, which are complex impedance (Z*), complex electric modulus (M*), which are related to each other:

$$Z^* = Z' - jZ'' = 1/j\omega C0\varepsilon^*$$

$$M^* = M' + jM'' = 1/\varepsilon^* = j\omega C0Z^*$$

Where (Z', M') and (Z'' M'') are the real and imaginary components of impedance and electrical modulus, respectively, $\omega=2\pi f$ is the angular frequency and $j=\sqrt{-1}$ is the imaginary factor. The complex impedance of "electrode/sample/electrode" configuration can be explained as the sum of a single Z_{CPE} with a parallel combination of R and CPE (R=resistance, CPE=constant phase element (CPE)) circuit. Z_{CPE} is usually considered as a dispersive capacitance, α is the measure of the capacitive nature of the element: if α=1, the element is an ideal capacitor, if α=0, it behaves as a frequency independent ohmic resistor. Thus, the impedance analysis is not ambiguous, and hence provides a clear and efficient graphical circuit analysis formalism to obtain "optimal" system.

Impedance analysis: Figures 9a and 9b show temperature dependence Nyquist Plots of the [Zn(dpc)Cl_2].H_2O measured at different temperatures [298-418K]. Moreover, it can be noticed that the complex impedance plots show that the arc of the semicircle lying below the real (Z') axis (resistance) can be developed as an overlapped contribution, which confirms the polydispersive (multi-cole-cole type) nature of dielectric relaxation in this compound. As the temperature increases to 343K, the semicircles move to a lower value of resistance and the Warburg contributions start diminishing until their complete disappearance. The effect disappears above this temperature, then return to a heat impedance value and change their forms at T=388K.

Electric modulus analysis: Electric modulus formalism is an important theory, set up by Macedo et al. [44]. It permits not only to examine the charge transport processes in ion conductors (such as mechanism of electrical transport, conductivity relaxation and ion dynamics as a function of frequency and temperature) but also to eliminate electrode polarization effect. The electric modulus (M*) is obtained from the above expression:

$$M^*(f) = M' + jM''$$

where $M^*(f) = M' + jM''$ and $M'' = \omega C0Z'$. Figure S4 shows the frequency dependence of the imaginary part of the electric modulus (M'') at different temperatures. The plot shows an asymmetric behaviour with respect to peak maxima. These spectra also reflect the motions of the hydrogen in the material by exhibiting two apparent relaxation regions. The left parts of the peak indicate the conduction process while the region on the right is associated with the relaxation process where the ion can be well localized.

Circuit model: The complex impedance spectroscopy is a technique characterizing the electrical behavior of a system in which a number of strongly coupled processes exist. It helps to separate bulk (grain), grain boundary (intergrain), electrode-solid interface polarization and Warburg phenomena contributing in the transport properties of the material [46]. Impedance data can be fitted and analyzed on the basis of an ideal circuit model with discrete electrical components [47]. The measurements of impedance give information on resistive (real part) and reactive (imaginary part) components in a material. Typical impedance curves are reported in Figure 10. All obtained impedance curves are well fitted with the unique equivalent circuit (R_b, CPE_b), (R_{gb}, CPE_{gb}), (R_i, CPE_i) and (R_w, CPE_w), where R_b, R_{gb} R_i and R_w represent the bulk, grain boundary, electrode-solid interface polarization and Warburg resistance, respectively; and CPE_b, CPE_{gb}, CPE_i and CPE_w represent the bulk, grain boundary, electrode-solid interface polarization and Warburg constant-phase elements respectively. If the Warburg effects are excluded, then the equivalent circuit can be modeled with three semi-circles in the impedance plane.

$$Z^*(\omega) = (\frac{1}{R_g} + j\omega C_g)^{-1} + (\frac{1}{R_{gb}} + j\omega C_{gb})^{-1} + (\frac{1}{R_{el}} + j\omega C_{el})^{-1} + R_s$$

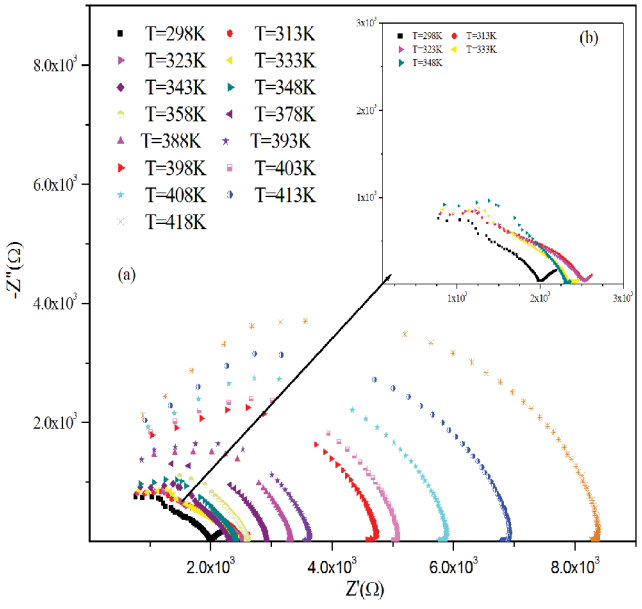

Figure 9: The impedance complex plots (a) at different temperatures and (b) at T = [298–348K] of the Zn(dpc)Cl_2.H_2O.

By means of electrochemical impedance spectroscopy, the bulk resistance (R_b) for the different effects can be evaluated. This parameter also provides us with information about the easiness of bulk at the compound and additionally includes the electrochemically active grain boundary, electrode-solid interface polarization and Warburg parameters, not considered in the rate constant information. In Figure 10, the impedance spectra of this hybrid are depicted. The parameter R_b is obtained by fitting the impedance spectra to a simple equivalent circuit and the well-known Randles circuit is depicted in Figure 10. In such equivalent circuit, the other parameters have the following meanings: R_s, R_{gb}, R_i and R_w represent the resistance of the other phenomena, CPE is the constant phase element associated with capacitance of the bulk, grain boundary, electrode-solid interface polarization and Warburg impedance associated with the diffusion of the electro active species. The quantitative values of the bulk part obtained after fitting were listed in Table S5.

Conductivity analysis: The electrical conductivity is a thermally activated process that follows the Arrhenius law. The activation energy for the conduction (Ea) of this sample could be calculated from log(σT) versus 1000/T plot. Figure 11 depicts the Arrhenius plots of the conductivity evaluated from the impedance plots of the sample as a function of temperature. The corresponding activation energy found before and after fitting and that of the relaxation energy according to the opposite temperature (1000/T) of the bulk part are represented in Figure S4.

The temperature dependence of the conductivity was studied and compared before and after fitting showing that the conductivity of the sample is influenced by the grain boundaries and the electrode interface phenomena. Within the framework of the studied temperature, there are three regions indicated as I, II and III separated at T=343K and T=388K. The values of the bulk conductivity obtained from the complex impedance semicircles Figure S4 in regions I, II and II are Ea1=0.03 eV, Ea2=0.04 eV and Ea3=0.07 eV, respectively. The peak frequency, f_{max}, for the bulk of this sample as a function of the inverse temperature

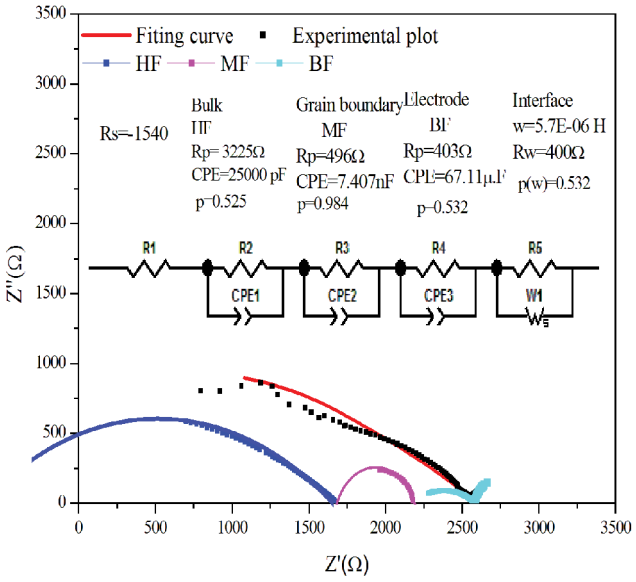

Figure 10: Complex impedance plane plots at 318 K and equivalent circuit mode of $Zn(dpc)Cl_2.H_2O$ compound. Impedance diagram obtained after fitting. Equivalent circuit used for modelling data presented in (A). The best fitting values are labeled as "fitted" in (A).

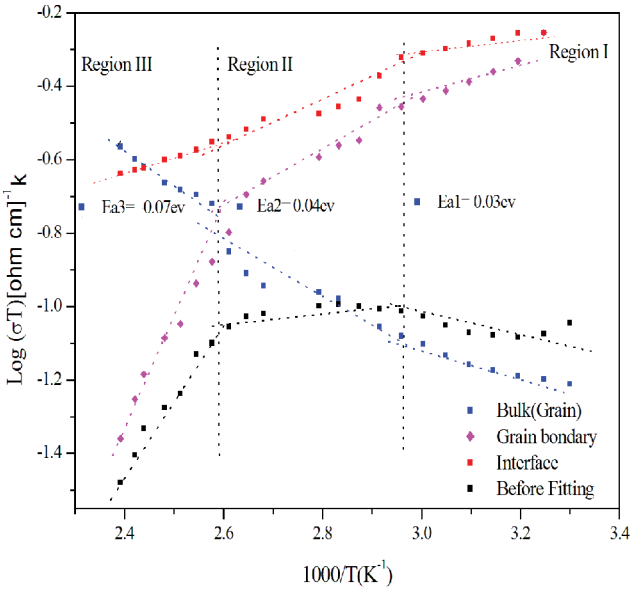

Figure 11: Dependence of log (σT) on temperature before and after fitting of $Zn(dpc)Cl_2.H_2O$ compound.

is shown in Figure S4. The figure reveals that for the corresponding sample, there is an activated relaxation process (Arrhenius-type) in the temperature range of 298-418K with three regions separated at T=343K and T=388K. The values of the relaxation energy of the bulk in regions I, II and III are Er1=0.04 eV, Er2=0.30 eV and Er3=0.09 eV. In both the two regions I and III, the relaxation energy values are close to the values of the conductivity obtained from the complex impedance for the same temperature as regions I and III. This result implies that the charge carrier has to overcome the same energy barrier while conducting and relaxing. But there is a difference in the values of Ea2 and Er2 for region II. In that case, the relaxation of region II is attributed to a reorientation of H_2O due to the water reorientations and the proton displacement according to Colomban-Novak classification [48]. Consequently, the thermogravimetric (ATG) results show one change of spawn at T=385K and the scanning differential calorimetric (DSC) results show two endothermic peaks: the first one at T=345K and the second at T=386K this is due to a phase transition at T=345K and loss of mass (departure of the water structure) at T=386K, which may be interpreted by the fact that the conductivity in the three mentioned regions are ensured by the hydrogen mobility. Therefore, and considering the discussed results in terms of the values of the relaxation energy in the region II, this could be attributed to H^+ jump and H_2O reorientation changing. In fact, the reorganization of the structural pattern or environment is an inherent part inside H_2O, which may explain the phase transition at T=345K.

Conclusion

The present work investigates the synthesis by slow evaporation at room temperature and explores physical–chemical properties of new organic-inorganic-zinc-chloride based on general formula $[Zn(C_7H_5NO_4)Cl_2].H_2O$. It appears that this compound, at room temperature, belongs to the orthorhombic system (space group *Pnna*). The crystal structure has been characterized by X-ray diffraction; Hirshfeld surface fingerprint plots show different types of intermolecular interactions including hydrogen bonding, Infrared and Raman spectroscopy studies that are consistent with the structure. Most of the organic and inorganic contributions to the vibrations

are identified. The NMR spectroscopy is proves to give a rather good insight of the chemical shift relative to ^{13}C. The dielectric properties of the title compound are investigated using complex impedance spectroscopy. The electrical properties of the reported compound are studied as a function of frequency and temperature in the ranges of 209 Hz-5 MHz and 298K-418 K, respectively. The previously studied dielectric properties present two anomalies at 343 and 388K. These anomalies are also detected by technical TGA and DSC, which could be attributed to a phase transition at T=343K and the disappearance of the water molecule of the structure at T=388K. The value of the activation energy of the grain part implies that the conduction is performed by a hopping of a proton H^+ and the value of the relaxation energy proves that this salt has the same mechanism of hopping. This material exhibits considerable conductivity at room temperature and is a possible candidate for electrode material in solid-state batteries.

Supplementary Material

Crystal data for a new complex containing: dipicolinic cation together with zinc chloride ligand, namely $Zn(C_7H_5NO_4)Cl_2.H_2O$ ($Zn(dpc)Cl_2.H_2O$), has been deposited at the Cambridge Crystallographic Data Center as supplementary publications (CCDC-977198). The data can be obtained free of charge from the Cambridge Crystallographic Data Center, 12 Union Road, Cambridge CB2 1EZ, UK, Fax: +441223336033; E-mail: deposit@ccda.cam.ac.uk.

Acknowledgements

The authors would like thank all members of the unit of common services, at the University of Sfax particularly Mr Tarek GARGOURI, for their valuable assistance and special support concerning the measurements of X-ray diffraction. The authors are also grateful to Prof Hamadi Khemakhem for his useful co-operation as far as the Raman spectroscopy measurement is concerned.

References

1. Mitzi DB, Chondroudis K, Kagan CR (2001) Organic-inorganic electronics IBM J Res Dev 45: 29-45.
2. Li Y, Zheng G, Lin C, Lin J (2007) Synthesis, structure and optical properties of different dimensional organic-inorganic perovskites. Solid State Sci 9: 855-861.
3. Aruta C, Licci F, Zappettini A, Bolzoni F, Rastelli F, et al. (2005) Growth and optical, magnetic and transport properties of $(C_4H_9NH_3)_2MCl_4$ organic-inorganic hybrid films (M = Cu, Sn). Appl Phys A 81: 963-968.
4. Zhang W, Ye HY, Cai HL, Ge JZ, Xiong RG, et al. (2010) Discovery of new ferroelectrics: [H2dbco]2 × [Cl_3] × [$CuCl_3(H2O)_2$] × H2O (dbco = 1,4-Diaza-bicyclo[2.2.2]octane). J Am Chem Soc 132: 7300-7302.
5. Pradeesh K, Agarwal M, Koteswara Rao K, Vijaya Prakash G (2010) Synthesis, crystal structure and optical properties of quasi-one-dimensional lead (II) iodide: $C_{14}H_{18}N_2Pb_2I_6$ Solid State Sci 12: 95-98.
6. Plowas I, Szklarz P, Jakubas R, Bator G (2011) Structural, thermal and dielectric studies on the novel solution grown (4-dimethylaminopyridinium) chloroantimonate(III) and chlorobismuthate(III) crystals. Mater Res Bull 46: 1177-1185.
7. Zdanowska-Fraczek M, Holderna-Natkaniec K, Fraczek ZJ, Jakubas R (2009) Molecular dynamics and electrical conductivity of $(C_3N_2H_5)_5Bi_2Cl_{11}$. Solid State Ion 180: 9-12.
8. Era M, Morimoto S, Tsutsui T, Saito S (1994) Organic-inorganic heterostructure electroluminescent device using a layered perovskite semiconductor $(C_6H_5C_2H_4NH_3)_2PbI_4$. Appl Phys Lett 65: 676-678.
9. Kagan CR, Mitzi DB, Dimitrakopoulos CD (1999) Organic-inorganic hybrid materials as semiconducting channels in thin-film field-effect transistors Science 286: 945-947.
10. Kazuhiro Y, Noriko Y, Tadayasu F (1994) Europ Patent 33: 2267-2272.
11. Burdock GA (1996) Encyclopedia of Food and Color Additives, CRC Press, New York, USA, p: 3.
12. Yang L, Crans DC, Miller SM, la Cour A, Anderson OP, et al. (2002) Cobalt(II) and cobalt(III) dipicolinate complexes: solid state, solution, and in vivo insulin-like properties. Inorg Chem 41: 4859-4871.
13. Sileo EE, Blesa MA, Rigotti G, Rivero BE, Castellano EE (1996) The crystal chemistry of copper(II) dipicolinates. Polyhedron 15: 4531-4540.
14. Ma C, Chen C, Liu Q, Liao D, Li L (2003) The First Structurally Characterized Trinuclear Dipicolinato Manganese Complex and its Conversion into a Mononuclear Species by Ligand Substitution. Eur J Inorg Chem 42: 1227-1231.
15. Wen LL, Dang DB, Duan CY, Li YZ, Tian ZF, et al. (2005) 1D helix, 2D brick-wall and herringbone, and 3D interpenetration d10 metal-organic framework structures assembled from pyridine-2,6-dicarboxylic acid N-oxide. Inorg Chem 44: 7161-7170.
16. Moghimi A, Sharif MA, Shokrollahi A, Shamsipur M, Aghabozorg H (2005) A Novel Proton Transfer Compound Containing 2, 6-Pyridinedicarboxylic Acid and Creatinine and its Zinc(II) Complex — Synthesis, Characterization, Crystal Structure, and Solution Studies. Z Anorg Allg Chem 631: 902-908.
17. Tabatabaee M, Aghabozorg H, Attar Gharamaleki J, Sharif MA (2009) Acridinium (6-carboxy-pyridine-2-carboxyl-ato)(pyridine-2,6-dicarboxyl-ato)zincate(II) penta-hydrate. Acta Crystallogr Sect E Struct Rep Online 65: m473-474.
18. Durkaya F, Dege N, Demirtas G, Ucar I (2011) Aqua-(di-2-pyridyl-amine-kN,N)(pyridine-2,6-dicarboxyl-ato-kO,N,O)zinc monohydrate. Acta Crystallogr Sect E Struct Rep Online 67: m687.
19. Kapetaniou EG, Braaz R, Jendrossek D, Papageorgiou AC (2005) Crystallization and preliminary X-ray analysis of a novel thermoalkalophilic poly(3-hydroxybutyrate) depolymerase (PhaZ7) from Paucimonas lemoignei. Acta Crystallogr Sect F Struct Biol Cryst Commun 61: 479-481.
20. Car IU, Bulut A, Karadag A, Kazak C (2007) J Mol Struct 61: 38-42.
21. McKinnon JJ, Jayatilaka D, Spackman MA (2007) Towards quantitative analysis of intermolecular interactions with Hirshfeld surfaces. Chem Commun (Camb) : 3814-3816.
22. Massiot D, Theile H, Germanus A (1994) WinFit—a Windows-based program for line shape analysis. Bruker Rep 140: 43-46.
23. Charlot G (1974) Chimie Analytique Quantitative, (Masson, Paris 1974), p: 2.
24. Sheldrick (1986) SHELXS-86, Program for Crystal Structure Solution, University of Gottingen (Germany 1986).
25. Sheldrick GM (1997) SHELXL-97, Program for Crystal Structure Refinement, University of Göttingen (Germany 1997).
26. Farrugia LJ (1997) ORTEP-3 for Windows - a version of ORTEP-III with a Graphical User Interface (GUI). J Appl Crys 30: 565.
27. Brandenburg K (1998) Diamond Version 2.0 Impact (Gbr, Bonn, Germany 1998).
28. Del Río I, Gossage RA, Hannu MS, Lutz M, Spek AL, et al. (2000) Synthesis and characterization of two new "pincer" complexes of zinc(II). The X-ray crystal structures of the five coordinate complexes [ZnCl2{η3-NN'N-2,6-(R2NCH2)2C5H3N}] (R = n-Bu or Me). Can J Chem 78: 1620-1626.
29. Addison AW, Rao TN, Reedijk J, van Rijn J, Verschoor GC (1984) Synthesis, structure, and spectroscopic properties of copper(II) compounds containing nitrogen–sulphur donor ligands; the crystal and molecular structure of aqua[1,7-bis(N-methylbenzimidazol-2′-yl)-2,6-dithiaheptane]copper(II) perchlorate. J Chem Soc, Dalton Trans 1984: 1349-1356.
30. Ghasemi K, Rezvani AR, Razak IA, Moghimi A, Ghasemi F, et al. (2013) Korean Chem Soc 34: 10-26.
31. McKinnon JJ, Spackman MA, Mitchell AS (2004) Novel tools for visualizing and exploring intermolecular interactions in molecular crystals. Acta Crystallogr B 60: 627-668.
32. Wolff SK, Grimwood DJ, McKinnon JJ, Turner MJ, Jayatilaka D, et al. (2012) CrystalExplorer (Version 3.0), University of Western Australia: Perth.
33. Can N, Sozerli Can SE, Atac A, Bardak F (2004) Structural characterization and luminescence properties of an isonicotinic acid N-oxide Mn(II) complex. Polyhedron 23: 1109-1113.
34. Can N, Atac A, Bardak F, Sozerli Can SE (2005) Spectroscopic and Luminescence Properties of an Isonicotinic Acid. Turk J Chem 29: 589-595.

35. Gudasi KB, Patil SA, Vadavi RS, Shenoy RV, Patil MS (2006) Synthesis and spectral studies of Cu(II), Ni(II), Co(II), Mn(II), Zn(II) and Cd(II) complexes of a new macroacyclic ligand N,N'-bis(2-benzothiazolyl)-2,6-pyridinedicarboxamide. J Serb Chem Soc 71: 529-542.

36. Karaa N, Hamdi B, Ben Salah A, Zouari R (2013) Synthesis, Infra-red, CP/MAS-NMR characterization, structural study and electrical properties of the bis(4-amino-2-chloropyridinium) tetrachlorozincate (II) monohydrate. J Mol Struct 1049: 48-58.

37. Massiot D, Fayon F, Capron M, King I, S Le Calvé, et al. (2002) Modelling one- and two-dimensional solid-state NMR spectra. Magn Reson Chem 40: 70-76.

38. Zielinski W, Rajca A (1995) Spectroscopic Methods for Organic Compound Identification.

39. Karaa N, Hamdi B, Oueslati A, Ben Salah A, Zouari R (2010) Synthesis, characterization and study of the chromogenic properties of the hybrid polyoxometalates $[PW_{11}O_{39}(SiR)_2O]^{3-}$ (R = Et, $(CH_2)_nCH= CH_2$ (n = 0, 1, 4), $CH_2CH_2SiEt_3$, $CH_2CH_2SiMe_2Ph$). J Inorg Organomet Polym 20: 746-754.

40. Quiroz-Castro E, Bernes S, Barba-Behrens N, Tapia-Benavides R, Contreras R, et al. (2002) Structural and spectroscopic characterisation of tris(2-benzimidazolylmethyl)amine coordination compounds of Zn(II), Cd(II) and Hg(II). Polyhedron 19: 1479-1484.

41. Karaa N, Hamdi B, Ben Salah A, Zouari R (2012) Synthesis, infra-red, MAS-NMR characterization, structural study and electrical properties of the new compound $[C_5H_6ClN_2]_2Cd_3C_{l8}$. J Mol Struct 1013: 168-176.

42. Maia LF, Rodrigues ACM (2004) Electrical conductivity and relaxation frequency of lithium borosilicate glasses. Solid State Ionics 168: 87-92.

43. Mogus-Milankovi A, Santi AS, Karabulut M, Day DE (2007) Study of electrical properties of MoO_3–Fe_2O_3–P_2O_5 and SrO–Fe_2O_3–P_2O_5 glasses by impedance spectroscopy. II. J Non-Cryst Solids 330: 128-141.

44. Macdonald JR (1987) Impedance Spectroscopy: Emphasizing Solid-State Material and Systems, Wiley: New York.

45. Venkataraman BH, Varma KBR (2003) Grain orientation and anisotropy in the physical properties of SrBi2 (Nb1− x V x) 2O9 (0≤ x≤ 0.3) ceramics. Mater Sci 38: 4895-4903.

46. Macedo PB, Moynihan CT, Bose R (1972) Role of ionic diffusion in polarization in vitreous ionic conductors. Phys Chem Glasses 13: 171-179.

47. Kumar S, Batoo KM, Prakash R, Choi HK, Koo BH, et al. (2010) Impedance spectroscopy study on $Mn_{1+x}Fe_{2-2x}Ti_xO_4$ (0≤x ≤0.5). J Cent South Univ Technol 17: 1133-1138.

48. Colomban PH, Novak A (1988) Proton transfer and superionic conductivity in solids and gels. J Mol Struct 177: 277-308.